TU Delft

Delft University of Technology

Document Version
Final published version

Licence
Dutch Copyright Act (Article 25fa)

Citation (APA)
Yao, M., Li, A., Ran, Z., Dong, X., Xiang, R., Chen, T., & Liu, G. (2026). Enhanced treatment of high-algae water and membrane fouling mitigation by SPDA@MIL-101-modified polyethersulfone ultrafiltration membranes with magnetic field regulation and magnetic flocculant assistance. *Journal of Environmental Chemical Engineering*, *14*(3), Article 122658. https://doi.org/10.1016/j.jece.2026.122658

Important note
To cite this publication, please use the final published version (if applicable).
Please check the document version above.

Copyright
In case the licence states “Dutch Copyright Act (Article 25fa)”, this publication was made available Green Open Access via the TU Delft Institutional Repository pursuant to Dutch Copyright Act (Article 25fa, the Taverne amendment). This provision does not affect copyright ownership.
Unless copyright is transferred by contract or statute, it remains with the copyright holder.

Sharing and reuse
Other than for strictly personal use, it is not permitted to download, forward or distribute the text or part of it, without the consent of the author(s) and/or copyright holder(s), unless the work is under an open content license such as Creative Commons.

Takedown policy
Please contact us and provide details if you believe this document breaches copyrights.
We will remove access to the work immediately and investigate your claim.

This work is downloaded from Delft University of Technology.

Journal of Environmental Chemical Engineering 14 (2026) 122658

Contents lists available at ScienceDirect

Journal of Environmental Chemical Engineering

journal homepage: www.elsevier.com/locate/jece

Enhanced treatment of high-algae water and membrane fouling mitigation by SPDA@MIL-101-modified polyethersulfone ultrafiltration membranes with magnetic field regulation and magnetic flocculant assistance

Meng Yao [a], Ang Li [b], Zhilin Ran [a,*], Xiaoqing Dong [a], Ruiyan Xiang [c], Ting Chen [d], Gang Liu [e,f]

[a] Shenzhen University of Information Technology, Shenzhen, Guangdong 518172, China
[b] Shenyang Jianzhu University, School of Municipal and Environmental Engineering, Shenyang, Liaoning 110168, China
[c] Dongguan University of Technology, Dongguan, Guangdong 523808, China
[d] Guangdong GDH Water Company Limited, Shenzhen, Guangdong 518021, China
[e] Delft University of Technology, Delft 2629, the Netherlands
[f] Research Center for Eco-Environmental Sciences, Beijing 100085, China

ARTICLE INFO

Keywords:
High-algae water
Ultrafiltration membrane material
Membrane fouling
Magnetic flocculant
Cake layer regulation

ABSTRACT

Harmful algal blooms threaten drinking water safety. Although ultrafiltration can effectively retain algae cells and algal-derived pollutants, such as extracellular polymeric substances, it still faces challenges such as severe membrane fouling and insufficient contaminant removal. To address these issues, this study developed an integrated "membrane material–flocculant–magnetic regulation" process to enhance algae-laden water treatment and mitigate fouling. Nanoparticles of sulfonated polydopamine (SPDA)-modified Materials of Institute Lavoisier-101 (MIL-101), denoted SPDA@MIL-101, were utilized to functionalize a polyethersulfone (PES) ultrafiltration membrane, enhancing its hydrophilicity and negative surface charge. Meanwhile, a magnetic flocculant (PCNF), composed of polyferric sulfate (PFS), sodium carboxymethyl cellulose (CMC-Na), and iron(II,III) oxide (Fe_3O_4) nanoparticles, was synthesized. Under an external magnetic field, a combined coagulation–ultrafiltration process was employed to actively regulate the cake layer, forming a magnetically responsive cake layer with a graded structure of lower density at the bottom and higher density at the top. The SPDA@MIL-101/PES membrane exhibited significantly improved hydrophilicity, indicated by the reduced contact angle of 54.89°, as well as excellent removal efficiency toward algae-derived fluorescent organic matter. Guided by the magnetic field, the PCNF flocculant formed a loose and porous cake layer, leading to a membrane flux recovery rate of 89% and a reduction in irreversible fouling to 11%. Mechanistic analysis revealed that the magnetic field-mediated dynamic reconstruction of the cake layer optimized the pore network, simultaneously improving contaminant retention and flux recovery performance. This study provides a feasible strategy for the treatment of high-algae water by combining material innovation and process regulation.

1. Introduction

In recent years, the frequent occurrence of algal blooms has emerged globally as a significant threat to drinking water safety [1]. Such events not only exacerbate eutrophication but also induce multiple water quality risks due to the complex nature of algae-derived pollutants, such as algal cells and extracellular organic matter (EOM). Microcystins released by algal cells during senescence have been confirmed to exhibit hepatotoxicity and tumor-promoting activity [2], while soluble microbial products, abundantly present in EOM, can contribute to the deterioration of natural water bodies [3]. Ultrafiltration technology, recognized for its physical sieving mechanism and non-phase-change operation, is regarded as an effective solution for treating algae-laden water [4,5]. This technology can efficiently retain intact algal cells and EOM via size exclusion, thereby reducing disinfectant demand and the risk of disinfection byproduct formation in subsequent treatment stages. However, existing ultrafiltration systems still face operational bottlenecks, including low organic rejection rates and severe membrane fouling [6]. The types and remediation of pollution components in high-algae water are listed in Table 1.

* Corresponding author.
E-mail address: zhilinran_sziit@163.com (Z. Ran).

https://doi.org/10.1016/j.jece.2026.122658
Received 11 February 2026; Received in revised form 8 April 2026; Accepted 10 April 2026
Available online 12 April 2026
2213-3437/© 2026 Elsevier Ltd. All rights are reserved, including those for text and data mining, AI training, and similar technologies.

Membrane materials are the core element of membrane separation technology, and their design has to be innovative to overcome the efficiency bottlenecks inherent to ultrafiltration technology [11,12]. To address the issue of low rejection rates associated with the intrinsic properties of ultrafiltration membranes, the fabrication of modified ultrafiltration membranes has emerged as a central strategy for improving rejection performance. Current mainstream modification approaches encompass hydrophilic polymer blending, surface grafting, nanoparticle doping, and functional coating deposition. Metal-organic frameworks (MOFs), which are highly porous nanostructures formed by the coordination of metal ions with organic linkers, exhibit unique crystalline topological structures, characterized by high specific surface areas, tunable architectures, and ease of functionalization, and have received significant attention in recent years. These properties enable MOFs to significantly enhance the hydrophilicity and filtration capacity of ultrafiltration membranes [13,14]. Within the research on MOF-based mixed matrix membranes (MMMs), the Zr-MOF University of Oslo-66 (UiO-66 (Zr)) and the Cr-MOF Materials of Institute Lavoisier-101 (MIL-101 (Cr)) have attracted considerable interest due to their exceptional aqueous stability. UiO-66 possesses a high specific surface area, excellent thermal and chemical stability, and a well-defined pore structure [15]. It has been extensively applied in areas such as oily wastewater treatment [16], removal of heavy metals from water [17], and organic pollutant degradation [18]. In contrast, MIL-101 (Cr), another prominent MOF material, is distinguished by its even larger specific surface area, superior acid/base stability, and tunable pore apertures. Notably, studies have indicated that MIL-101 outperforms UiO-66 in enhancing membrane porosity and fouling resistance [19]. While research with a specific focus on using MIL-101 as filler for MMMs remains relatively limited, it has demonstrated great potential for this purpose, particularly for breaking the permeability-selectivity trade-off and mitigating membrane fouling.

Although the direct incorporation of MOFs into the polymer matrix of a membrane can significantly enhance contaminant rejection, several key challenges remain for their application. Firstly, the poor interfacial compatibility between MOFs and the polymer matrix may lead to defect formation at the interface, thereby compromising overall membrane performance. Furthermore, while the inherently high specific surface area and porosity of MOF materials can provide additional transport pathways, these properties simultaneously increase the risk of particle aggregation [20–23]. Consequently, effectively preventing MOF particle aggregation and optimizing their dispersion constitute a primary research focus. Dopamine, a small molecule inspired by mussel adhesive proteins, possesses unique adhesive capabilities, enabling it to adhere to both organic and inorganic surfaces, which also facilitates the formation of a polydopamine (PDA) surface layer [24]. Due to its organic backbone and abundant functional groups, PDA can form intermolecular and covalent bonds with various polymeric membrane substrates. These interactions not only enhance compatibility with the polymer matrix but also improve hydrophilicity and electronegativity. These properties collectively contribute to significantly enhanced fouling resistance of the membrane [25–27]. Building upon this foundation, hydrophilic polyethersulfone (PES) ultrafiltration membranes were fabricated by incorporating sulfonated PDA (SPDA)-modified MIL-101 (SPDA@-MIL-101) nanomaterials into the PES matrix via a phase inversion process.

Although intrinsic modifications of membrane materials have demonstrated significant efficacy in removing algae-derived pollutants, membrane fouling remains an inevitable challenge when applying standalone membrane separation technology in the treatment of algae-laden water [28,29]. This issue constitutes a key bottleneck constraining long-term operational stability. Studies have shown that coupling coagulation as a pretreatment step with membrane separation can effectively mitigate membrane fouling through synergistic effects [30]. Among coagulants, Fe-based salts not only exhibit excellent algal removal performance but also facilitate the formation of a loose, porous cake layer. This layer effectively intercepts small molecular substances that could potentially block membrane pores [31–33]. Sodium carboxymethyl cellulose (CMC-Na), as a natural anionic polymer, is characterized by abundant carboxylate ($-COO^-$) and hydroxyl (-OH) functional groups along its molecular chains. These functional groups play a dual role. Firstly, they form stable complexes with the hydrolyzed species of polyferric sulfate (PFS) through COO-Fe coordination bonds, thereby enhancing the structural stability of the composite; secondly, positioned on the extended long chains of CMC, the functional groups facilitate an effective spatial bridging effect among destabilized particles, promoting the formation of large-sized and robust flocs with improved separation efficiency. In recent years, CMC has demonstrated significant application potential in the development of high-performance coagulants [34]. Concurrently, magnetic nanomaterials have attracted widespread attention due to their unique small-size effects and large specific surface areas. In particular, iron(II,III) oxide (Fe_3O_4) nanoparticles are frequently employed in water treatment applications for the adsorption and recovery of heavy metals and organic compounds due to their superior adsorption capabilities [35]. Building on these findings, this study synthesized a novel magnetic composite flocculant, denoted PCNF, using Fe_3O_4 nanoparticles as the nucleation core. The synthesis leveraged the mechanisms of electrical double layer compression and adsorption bridging provided by PFS and employed a hydrothermal preparation method.

Although Fe-based coagulants can retain algae-derived pollutants by forming a porous cake layer, regulating the pore structure of this layer in

Table 1
Types and remediation of pollution components in high-algae water.

Feed solution	Pollutant type	Fouling mechanism	Interaction	Cleaning mode	References
Algal cell suspension	Algal cells	Cake layer	Size exclusion	Reversible fouling, removable by physical cleaning	[7]
Algal cell and debris suspension	Algal cells	Cake layer	Size exclusion	For reversible and irreversible fouling, effective removal can be achieved through physical flushing and chemical cleaning with agents, respectively.	[8]
	Cell debris	Pore blockage	Size exclusion		
DOM solution	Biopolymer substances	Cake layer	Size exclusion	For reversible and irreversible fouling, effective removal can be achieved through physical flushing and chemical cleaning with agents, respectively.	[9]
	Low molecular weight (LMW) molecules	Pore blockage	Hydrogen bonding, hydrophobic adsorption, and electrostatic repulsion.		
Algal suspension	Algal cells and debris	Cake layer	Size exclusion	For reversible and irreversible fouling, effective removal can be achieved through physical flushing and chemical cleaning with agents, respectively.	[10]
	Algal cells and debris	Cake layer	Size exclusion		
	Biopolymer substances	Pore blockage	Hydrogen bonding		
	Low molecular weight (LMW) molecules	Pore constriction	Hydrophobic interaction, polymer entanglement, and electrostatic repulsion		

situ remains difficult in the conventional coagulation–ultrafiltration process. While a loose structure reduces transmembrane pressure, it exacerbates the penetration risk of low-molecular-weight EOM [36]; conversely, a dense structure improves retention efficiency but leads to a sharp increase in hydraulic resistance [37,38]. This inherent trade-off between retention and flux fundamentally stems from the lack of effective in situ regulation methods for the pore structure of the cake layer in current processes. As a result, the functionality of the cake layer is confined to a static optimization state where improvements in one aspect come at the expense of another, posing a fundamental challenge that constrains further enhancements in process performance.

In response to the aforementioned bottlenecks, this study breaks through the traditional "passive interception" framework and proposes a magnetic field-mediated active regulation strategy for filter cake control. By introducing the magnetic flocculant PCNF, with Fe_3O_4 nanoparticles as the magnetic core, its spatially directional property [39] is leveraged to construct hydrophilic pollutant aggregates with magnetic units as the skeleton during the coagulation stage. Under the induction of an external magnetic field, these aggregates undergo orderly arrangement on the membrane surface, forming an axial-gradient filter cake characterized by a dense upper layer for interception and a loose lower layer for water permeation, thereby enabling the reconstruction and optimization of the pore network. Ultimately, this study establishes an integrated "active coagulation-ultrafiltration-magnetic field regulation" process, aimed at synergistically enhancing the removal efficiency of algae-derived pollutants and membrane fouling resistance. This work lays a solid foundation for the future development of water supply safety technologies and provides new insights and approaches for addressing water pollution challenges.

2. Materials and methods

2.1. Main reagents and instruments

Materials: PES (M_n = 100,000, BASF, Germany); N-methylpyrrolidone (NMP, Aladdin, China); polyvinylpyrrolidone (PVP K30, Zhonglian, China); PFS (Huasheng, China); CMC-Na (ZhanYun, China); PDA (Macklin, China); Tris-HCl buffer (Aimeimanni, China); ferrous sulfate heptahydrate (Macklin, China); ammonia solution (Macklin, China); chromium(III) chloride hexahydrate ($CrCl_3{\cdot}6H_2O$, Aladdin, China); terephthalic acid (PTA, Aladdin, China); 3-mercapto-1-propanesulfonate sodium salt (98%, Aladdin, China). All reagents were of analytical grade.

Main instruments: field emission scanning electron microscope (Gemini 300, Zeiss, Germany); X-ray photoelectron spectrometer (EscaLab Xi+, Thermo Fisher Scientific, USA); Fourier transform infrared (FTIR) spectrometer (Invenio S, Bruker, Germany); scanning electron microscope (MIRA LMS, Tescan, Czech Republic); atomic force microscope (Dimension Icon, Bruker, Germany); contact angle goniometer (LSA 100, Lauda Scientific, Germany); solid surface zeta potential analyzer (SurPASS, Anton Paar, Austria); UV–vis spectrophotometer (T6 New Century, China); flocculation test stirrer (ZR4–6, Zhongrun Water Industry Technology Development Co., China); fluorescence spectrophotometer (F7000, Hitachi, Japan).

2.2. Preparation and analysis methods for SPDA@MIL-101/PES membranes

MIL-101 was synthesized according to the method reported by Ali et al. [40]: 2.66 g $CrCl_3{\cdot}6H_2O$ and 1.66 g PTA were separately dissolved in 45 mL deionized water. The mixtures were combined and reacted at 210 °C for 12 h. The resulting green product was collected by centrifugation and alternately washed three times with deionized water and ethanol, followed by vacuum drying at 80 °C overnight to obtain purified MIL-101.

SPDA@MIL-101 was prepared via an in situ polymerization strategy: 0.1 g MIL-101 was ultrasonically dispersed in 60 mL of a 1:1 (v/v) water-ethanol mixture. Then, 0.1 g dopamine hydrochloride was added, followed by the introduction of 20 mL Tris-HCl buffer (0.01 M, pH 8.5) to initiate polymerization for 12 h. Subsequently, 3-mercapto-1-propanesulfonate was added, and the reaction continued for another 12 h. The final SPDA@MIL-101 composite was obtained after centrifugation and vacuum drying.

Finally, pre-dried PES powder, 1 wt% PVP, and SPDA@MIL-101 in varying mass ratios were homogeneously dispersed in NMP solvent. The mixture was subjected to ultrasonication for 30 min, followed by magnetic stirring for 12 h to form a stable casting solution. After degassing for 12 h, the solution was cast onto a glass substrate using a 150-μm doctor blade, and the loaded substrate was immediately immersed in deionized water for phase inversion. The membrane was solidified through periodic water exchange (every 12 h) to complete the phase separation process. The compositions of the casting solutions are summarized in Table 2.

The membrane porosity and mean pore size were determined using the gravimetric method. A wet membrane sample (4 cm^2) was first weighed and then dried at 100 °C for 12 h. The porosity (ε) was calculated according to Eq. (1).

$$\varepsilon = \frac{W_1 - W_2}{\rho A l} \times 100\% \tag{1}$$

where W_1 and W_2 represent the weights (g) of the wet and dry membranes, respectively, ρ is the density of water (g/cm^3), A is the membrane area (cm^2), and l is the membrane thickness (cm).

The mean pore size r of the membrane was calculated using the Guerout-Elford-Ferry equation, provided in Eq. (2).

$$r = \frac{\sqrt{(2.9\text{-}1.75\varepsilon) \times (8\eta l Q)}}{\varepsilon A \Delta P} \tag{2}$$

where η is the viscosity of water (Pa·s), Q is the volumetric flow rate of permeate water (m^3/s), and ΔP is the operating pressure (Pa).

2.3. Preparation method of magnetic PCNF flocculant

A total of 2.3 g ferrous sulfate heptahydrate and 4.6 g ferric chloride hexahydrate were dissolved in 120 mL deionized water. Under nitrogen protection, 20 mL of a 25% ammonia solution was slowly added to adjust the pH to 7, followed by reaction in a water bath at 60 °C for 30 min. The resulting product was washed, vacuum-dried at 60 °C, and ground to obtain Fe_3O_4 nanoparticles. Subsequently, 1.0 g CMC-Na was dissolved in 200 mL deionized water under stirring at 500 rpm at 35 °C for 30 min. An appropriate amount of aqueous PFS solution was added, and stirring continued for another 30 min. Meanwhile, 1.0 g of Fe_3O_4 nanoparticles was ultrasonically dispersed for 15 min and then added to the above mixture. After stirring for 30 min and an additional ultrasonication treatment, the mixture underwent natural aging for 24 h, followed by drying at 60 °C, grinding, and sieving through a 200-mesh sieve, ultimately yielding the PCNF composite flocculant.

2.4. Synergistic coagulation-ultrafiltration-external magnetic field treatment system

The experimental setup for the treatment of high-algae water is illustrated in Fig. 2. The coagulation system employed a cylindrical vessel with a diameter of 10 cm, a height of 25 cm, and an effective volume of 1 L. A dead-end ultrafiltration cell (76 mm in diameter) with a maximum filtration capacity of 400 mL was used, and a permanent NdFeB magnet was placed at the bottom of the ultrafiltration cup to provide an external magnetic field, with a distance of 10 mm between the magnet and the ultrafiltration membrane. The magnetic field intensity was calibrated and measured prior to the experiment using a handheld Lake Shore Model 410 gauss meter (equipped with a

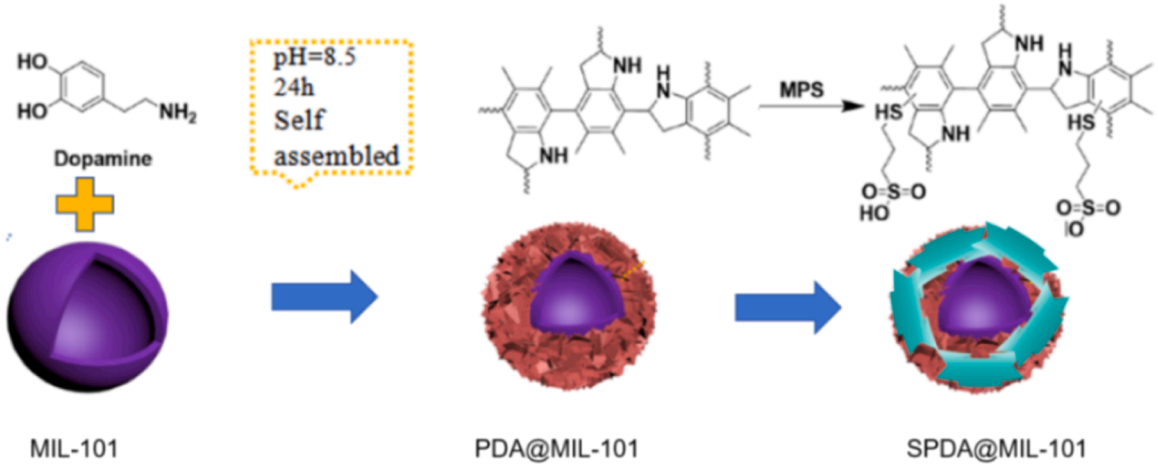


Fig. 1. Schematic diagram of the preparation mechanism of nanomaterials.

Table 2
Composition of different ultrafiltration membrane casting solutions.

Membrane	PES/(wt %)	PVP/(wt %)	NMP/(wt %)	SPDA@MIL-101/(wt %)
M0	16	1	83	—
M1	16	1	82.95	0.05
M2	16	1	82.90	0.1
M3	16	1	82.85	0.15
M4	16	1	82.80	0.2

transverse Hall probe). The ultrafiltration membrane had a diameter of 76 mm, and filtration was driven by a nitrogen pressure of 0.1 MPa. All filtration experiments were conducted under constant temperature conditions (room temperature 25 ± 1 °C) to avoid the influence of temperature fluctuation on the flux measurement.

To evaluate the antifouling performance of the ultrafiltration membrane, three cycles of filtration experiments were conducted by alternately filtering deionized water and high-algae water. The specific procedure for each cycle was as follows. First, 200 mL deionized water was filtered at 0.1 MPa to determine the initial flux. Subsequently, the feed solution was replaced with 300 mL high-algae water, and the flux variation was recorded until the end of filtration. Then, the membrane surface was rinsed in situ with deionized water using a gooseneck wash bottle. After rinsing, the feed solution was switched back to deionized water, and the next cycle commenced. This procedure was repeated three times. Based on the filtration data obtained from the three cycles, the flux recovery ratio (FRR), irreversible fouling ratio (R_{ir}), reversible fouling ratio (R_r), and total fouling ratio (R_t) were calculated according to Eqs. (3)-(6).

$$FRR = \frac{J_{s4}}{J_0} \times 100\% \tag{3}$$

$$R_{ir} = \frac{J_0 - J_{s4}}{J_0} \times 100\% \tag{4}$$

$$R_t = \frac{J_0 - J_{e3}}{J_0} \times 100\% \tag{5}$$

$$R_r = (R_t - R_{ir}) \times 100\% \tag{6}$$

3. Results

3.1. Characterization of mixed matrix membranes

The morphology and structure of MIL-101 and SPDA@MIL-101 were characterized by scanning electron microscopy (SEM), as shown in

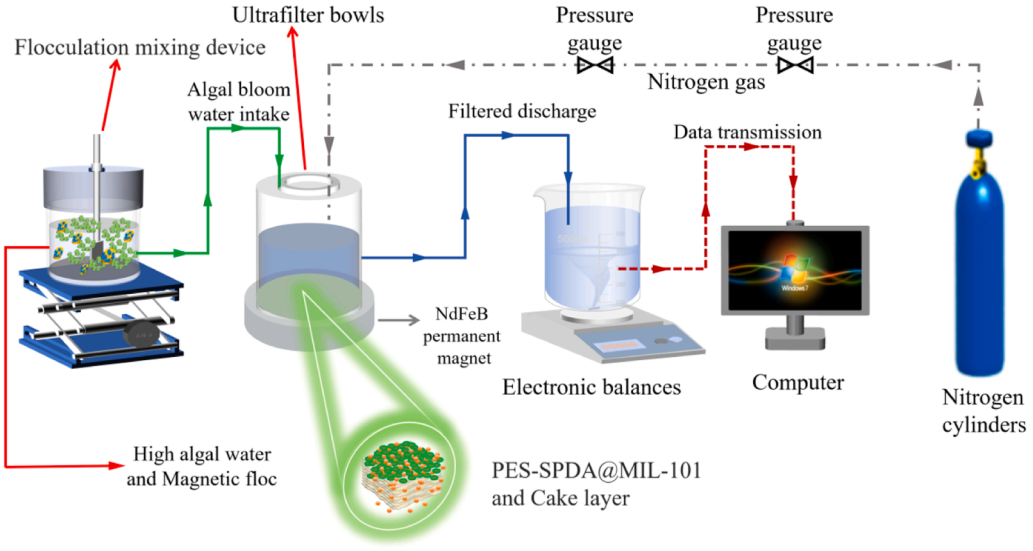


Fig. 2. Schematic diagram of the coupled coagulation-ultrafiltration-external magnetic field treatment device.

Fig. 3. Pure MIL-101 exhibited a typical octahedral morphology (Fig. 3a) with a particle size distribution in the range of 200–300 nm, indicating well-defined crystallinity and regular crystal structure [41]. SPDA@MIL-101 (Fig. 3b) maintained a similar octahedral structure and particle size range, but its surface became rougher due to the formation of a nanoscale polymer shell from SPDA coating, resulting in rougher lattice planes. This morphological difference confirmed that SPDA modification effectively altered the structural characteristics of the material surface.

Fig. 3c displays the zeta potential characteristics of the three nanoparticle materials. MIL-101 (Cr) showed positive surface charges under neutral conditions, attributed to the protonated metal-OH groups formed by surface Cr sites. To address the interfacial compatibility challenges caused by this positive charge when preparing negatively charged MMMs, the MOF was modified with SPDA, resulting in significant electronegativity enhancement of the obtained SPDA@MIL-101. The sulfonic acid groups (–SO_3H) introduced by SPDA can readily dissociate in water, effectively increasing the surface negative charge density of the material while enhancing its hydrophilicity and ion exchange capacity. This provides more hydrophilic and electronegative surface functional groups for subsequent membrane formation, thereby improving membrane performance.

Fig. 4 presents the elemental mapping analysis based on energy-dispersive X-ray spectroscopy (EDS), clearly revealing the chemical composition characteristics of MIL-101 and its derivative SPDA@MIL-101. The EDS results demonstrated that the crystalline framework of pristine MIL-101 consisted of Cr, O, and C elements, where Cr atoms coordinated with terephthalate ligands as trinuclear clusters to form characteristic octahedral structures, while O and C elements primarily originated from the organic ligand framework [42]. After modification by SPDA coating, distinct characteristic signals of N and S elements appeared on the material surface, showing a uniform distribution that closely corresponded to the MIL-101 particle morphology. Combined with the chemical features of amino (–NH_2) and SO_3H groups in SPDA molecules, this elemental distribution change confirmed the successful surface modification of MIL-101 through covalent bonding with the SPDA coating.

X-ray photoelectron spectroscopy (XPS) analysis (Fig. 5a) revealed binding energy shifts of the characteristic N 1 s (399.5 eV) and S 2p (168.5 eV) peaks, confirming the successful anchoring of SO_3H groups on the material surface. The splitting of the S 2p peak further indicated the formation of stable covalent linkages between SO_3H groups and the PDA backbone [43],reflecting favorable interfacial bonding of the SPDA coating. This stable surface chemistry originated from the synergistic effect between the inherent adhesion properties of PDA and the strong charge interactions of SO_3H groups, providing a reliable interfacial foundation for subsequent functional applications.

FTIR analysis (Fig. 5b) revealed characteristic absorption peaks at 1018 cm^{-1} and 748 cm^{-1} , corresponding to in-plane stretching and out-of-plane bending vibrations of aromatic C–C bonds, respectively, associated with the π-π conjugation in the aromatic structure of the material. The characteristic peak at 586 cm^{-1} was attributed to Cr–O stretching vibrations. Notably, the strong absorption at 1168 cm^{-1} corresponded to the asymmetric stretching vibration of SO_3H groups, consistent with the typical vibration modes of SO_3H groups in lignosulfonates (1200–1150 cm^{-1}). The broad absorption band observed at around 3400 cm^{-1} was attributed to the combined stretching vibrations of OH and NH_2 groups in dopamine molecules [44]. These results collectively confirmed the successful chemical modification of SPDA nanoparticles.

Fig. 6 illustrates the influence of nanomaterial loading on the surface morphology and roughness of ultrafiltration membranes. At loadings below 0.1 wt% (M1, M2), SEM images revealed uniform and smooth surface structures, attributable to the enhanced compatibility between the membrane matrix and nanoparticles imparted by PDA. However, exceeding the critical threshold of 0.1 wt% (M3, M4) resulted in nanoparticle aggregation. Analysis of atomic force microscopy (AFM) images (Fig. 6) indicated a nonlinear trend in surface roughness, initially decreasing and then increasing with the loading amount of the nanomaterial. The high hydrophilicity of the nanoparticles accelerated phase separation, initially generating smoother surfaces. Subsequent roughness increase originated from elevated casting solution viscosity due to nanoparticle addition, which impeded phase separation and promoted nanoparticle aggregation, consequently increasing the surface roughness of the membrane [45].

In cross-sectional SEM images (Fig. 6), all membranes exhibited a typical three-layer heterogeneous structure: a macroporous support layer at the bottom, an intermediate finger-like pore transition layer, and a dense sponge-like functional layer at the top [45]. With nanoparticle incorporation (M0→M2), altered phase separation kinetics facilitated the transition of pore channels from oblique to vertical alignment, forming interconnected straight-pore structures that effectively reduced fluid transport resistance. However, when the nanoparticle concentration exceeded the critical value (≈0.1 wt%, M2→M4), particle aggregation caused pore channels to revert to oblique orientations, albeit with some improvement in the underlying void structure and the mechanical properties of the membrane. This structural

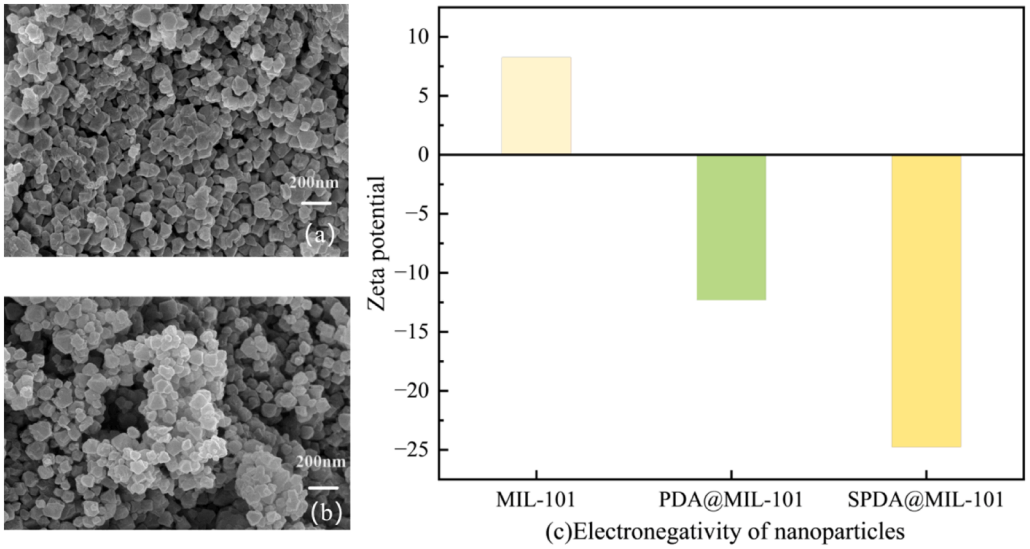


Fig. 3. (a, b) SEM images of nanoparticle materials and (c) their electronegativity analysis diagram.

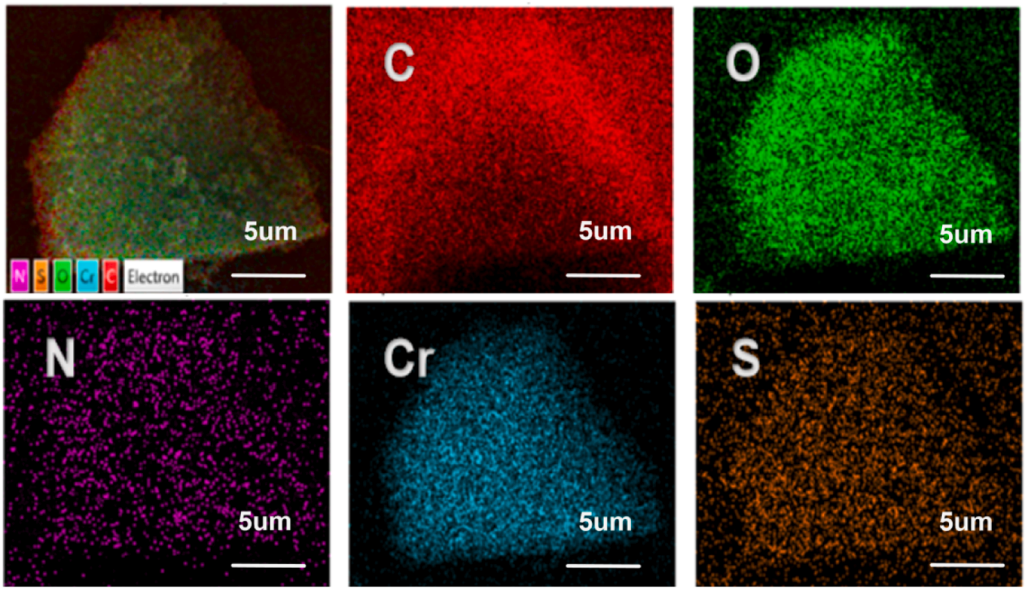


Fig. 4. EDS mapping images of SPDA@MIL-101.

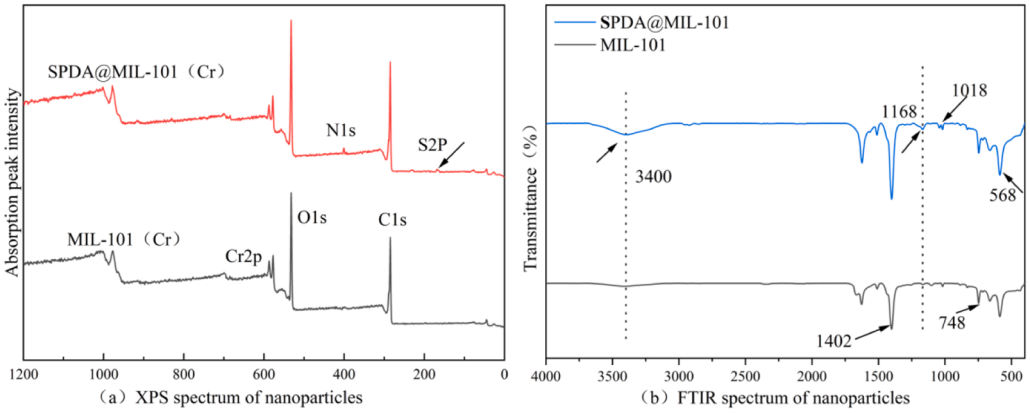


Fig. 5. XPS and FTIR spectra of MIL-101 and SPDA@MIL-101.

evolution indicates the existence of a critical dispersion concentration for nanoparticles in membranes. Below this threshold, nanoparticles act as topological modifiers, optimizing the pore structure; beyond it, they form physical cross-linking points that enhance fracture toughness through a sacrificial bond mechanism. This finding provides theoretical guidance for designing composite membranes with simultaneous high flux and mechanical stability.

3.2. *Performance analysis of mixed matrix ultrafiltration membranes*

As evident from the data provided in Table 3, increasing the PDA@MIL-101 nanoparticle loading from 0 wt% to 0.1 wt% significantly enhanced the membrane porosity from 45% (M0) to 62% (M2), representing a 37.8% improvement. All modified membranes exhibited a mean pore size of 42–44 nm, approximately 4.4% smaller than that of M0, attributed to an accelerated phase separation process. Thus, moderate nanoparticle addition optimized the pore channel structure of the membrane through interfacial effects that induced secondary pore formation during phase separation. However, exceeding the critical nanoparticle concentration led to increased casting solution viscosity due to particle aggregation, which hindered solvent diffusion and compromised pore connectivity. Cross-sectional SEM analysis further confirmed that the M2 membrane possessed an interconnected multilevel pore structure, while highly-loaded samples (e.g., M4) exhibited densified regions. In summary, the M2 membrane, with a mean pore size of 42.82 nm and a porosity of 62%, demonstrated superior permeation selectivity, providing a structural foundation for subsequent antifouling research.

The surface hydrophilicity and interfacial charge characteristics of the ultrafiltration membranes are analyzed in Fig. 5. The unmodified M0 membrane exhibited a static water contact angle of 71.28°. With increasing incorporation of SPDA@MIL-101 nanoparticles, the contact angle showed a nonlinear trend, initially decreasing and then increasing (Fig. 7a). The M2 membrane achieved the lowest contact angle of 54.89°, representing a 22.99% reduction compared to M0, primarily attributed to the enhanced surface hydrophilicity imparted by the SO_3H and OH groups in SPDA. The improved hydrophilicity not only reduces water-membrane interfacial tension to facilitate water permeation but also forms a dense hydration layer that effectively mitigates the adsorption of hydrophobic pollutants.

Zeta potential measurements (Fig. 7b) revealed that all membranes had negative surface charges at pH 7. Across the pH range of 5–9, the unmodified M0 membrane showed a potential decrease from −19 mV to −41 mV, while the SPDA@MIL-101-modified M2 membrane demonstrated a more substantial decline from −21 mV to −60 mV. The negative charge density on the surface of M2 was 1.77 times that of the

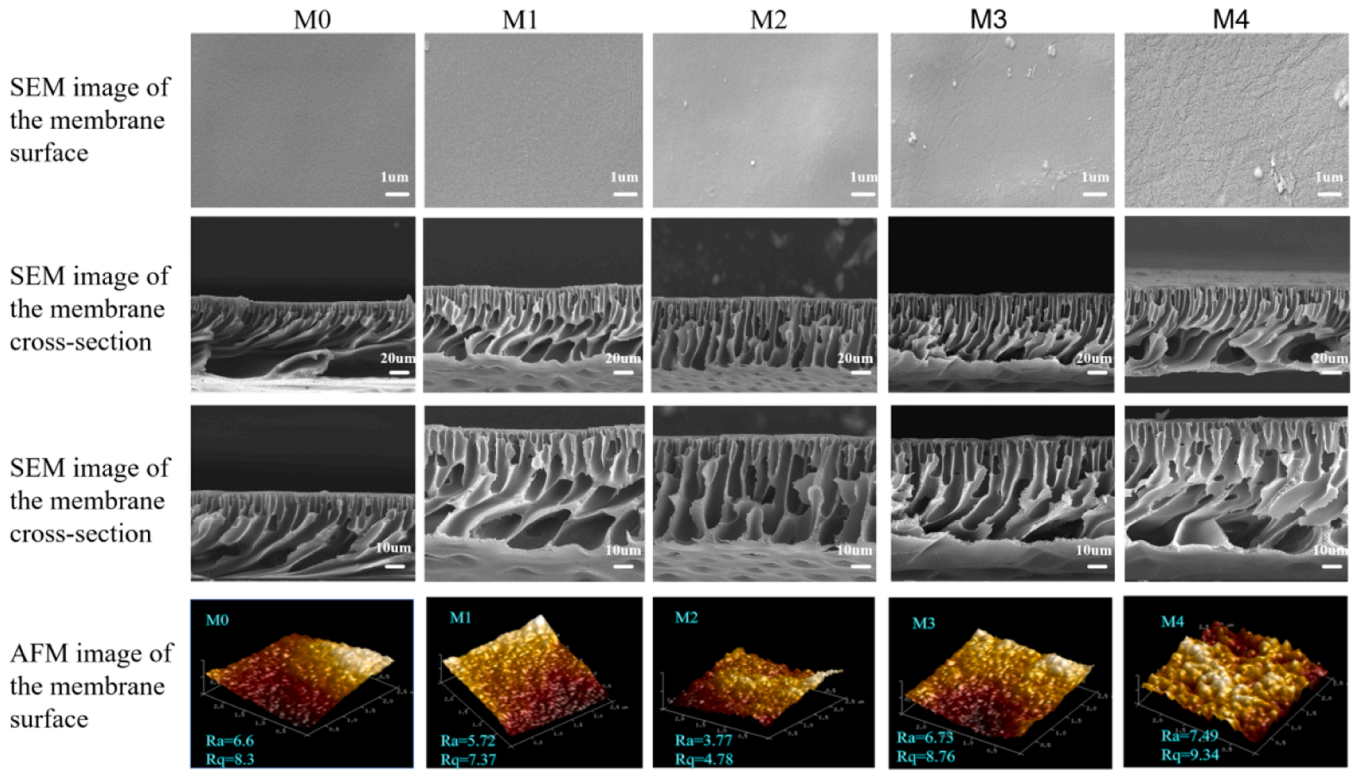


Fig. 6. Surface morphology and structure analysis of ultrafiltration membranes with different nanoparticle additions.

Table 3
Porosity and average pore size of five types of ultrafiltration membranes.

Membrane	Porosity (%)	Average pore size (nm)	MWCO (kDa)
M0	45	43.87	97
M1	50	42.96	90
M2	62	42.82	79
M3	55	42.49	87
M4	52	42.84	94

M0 surface, mainly due to the synergistic effect between the strong ionization capability of SO_3H groups and the presence of OH groups [46]. The enhanced electronegativity effectively reduces the deposition of negatively-charged algal pollutants on the membrane surface through electrostatic repulsion.

3.3. Removal efficiency analysis of SPDA@MIL-101/PES mixed matrix membranes for algae-laden water treatment

Fluorescent organic substances in algae-laden water represent significant foulants in ultrafiltration processes. The SPDA@MIL-101-modified ultrafiltration membrane demonstrated removal of these fluorescent organics, effectively mitigating irreversible membrane fouling. Three-dimensional excitation-emission matrix (3D-EEM) spectra (Fig. 8b–e) revealed a prominent peak in Region IV (soluble microbial by-products) of the raw water. The M2 membrane with a 0.1-wt% nanoparticle loading achieved a reduction in the integrated fluorescence signals in this region, indicating effective retention of algal-derived soluble metabolites. The removal of protein-like substances (Regions I and II) exhibited a volcano-shaped trend with increasing nanoparticle content, with notable removal at a nanoparticle loading of 0.1 wt% (M2). Furthermore, characteristic blue shifts were observed in Region III (fulvic-like acids) and Region V (humic-like acids) after

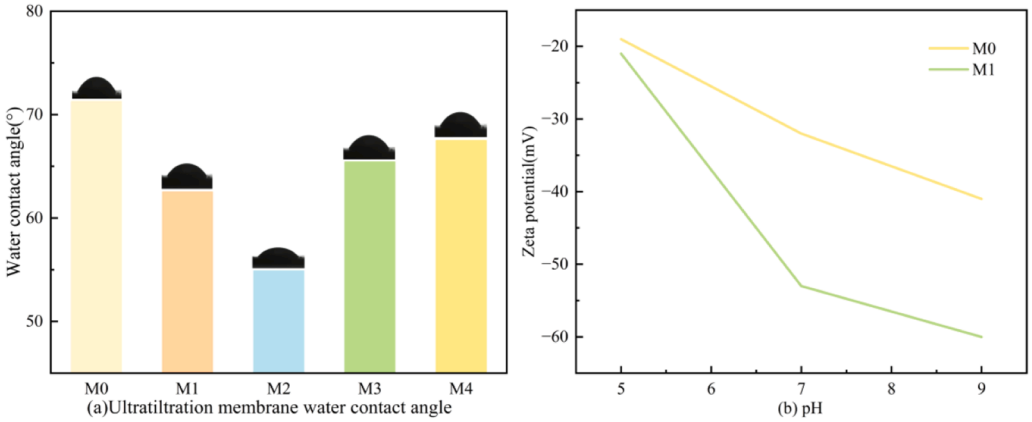


Fig. 7. Hydrophilicity and electronegativity of membrane materials with different mass ratios.

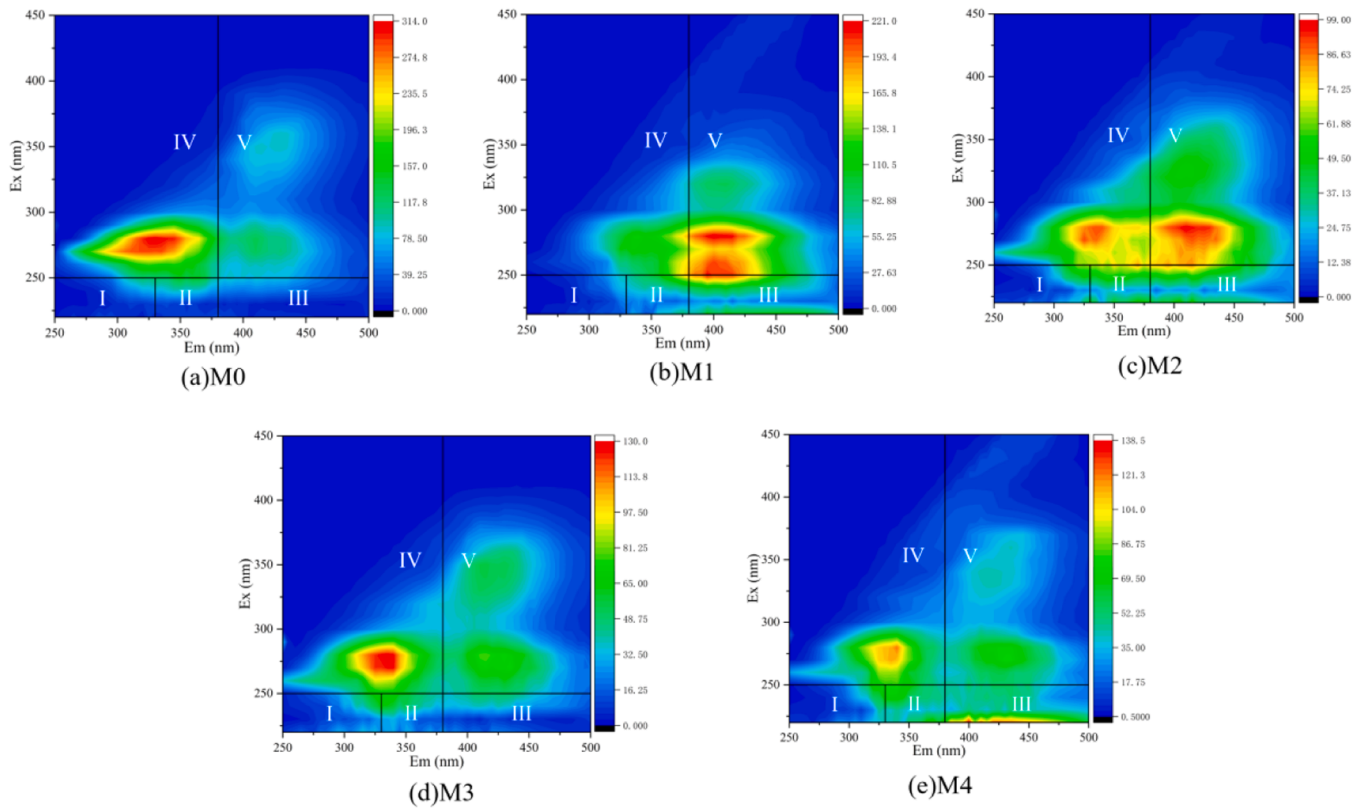


Fig. 8. Three-dimensional fluorescence analysis of high-algal water post-filtration using SPDA@MIL-101-modified ultrafiltration membranes with different mass ratios.

treatment with the M2 membrane, confirming its removal capability for humic substances.

To systematically evaluate the antifouling performance of the ultrafiltration membranes, this study examined the flux evolution patterns of five modified membranes with different mass ratios through three consecutive filtration cycles in both algae-laden water and pure water systems (Fig. 9a). The algae-laden water system exhibited a continuous flux decline due to interactions between algal cell secretions and the membrane surface, with significantly lower flux compared to the pure water system. This observation suggested that small-molecule pollutants contributed to flux reduction through membrane pore blockage, while large-molecule pollutants exacerbated fouling via cake layer formation, which was particularly evident for the unmodified M0 membrane. The modified membranes (e.g., M2), with straighter pore structure and enhanced hydrophilicity, demonstrated significantly improved pure water flux compared to M0, effectively mitigating pollutant deposition.

Flux recovery rate tests (Fig. 9b) revealed substantially enhanced antifouling performance in the modified membranes. The M2 membrane achieved a recovery rate of 89% after three cycles, representing a 17% improvement over M0 (72%). The variation in recovery rate closely correlated with the evolution of membrane hydrophilicity. The enhanced hydrophilicity and electronegativity of the modified membranes promoted the formation of a hydration layer, reducing the probability of pollutant-membrane contact while strengthening the electrostatic sieving effect [47]. The irreversible fouling index was 28% for M0 and only 11% for M2, representing a 17% reduction and

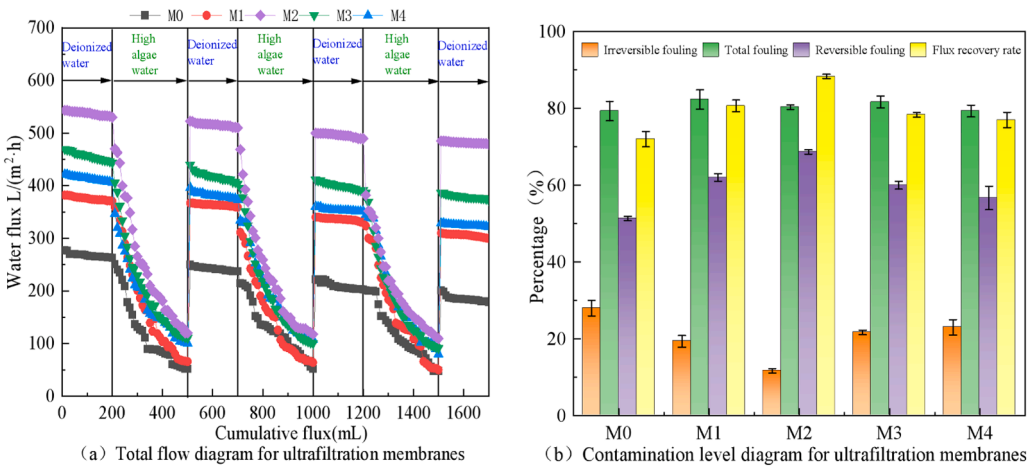


Fig. 9. Total flow diagram over three cycles of high-algal water treatment (a) and fouling and flux recovery rate diagram (b) for different ultrafiltration membranes.

confirming the effectiveness of nanoparticle modification.

3.4. Effect of coupling SPDA@MIL-101/PES mixed matrix membrane with PCNF magnetic flocculation on high-algal water treatment efficiency

Given the complex composition of pollutants in algae-laden water, membrane modification alone remains insufficient to prevent rapid flux decline during ultrafiltration, therefore requiring the integration of a pretreatment step. This study adopted a coagulation-ultrafiltration hybrid process to further mitigate reversible fouling and enhance organic pollutant retention. Leveraging the excellent magnetic responsiveness, large specific surface area, and biocompatibility of Fe_3O_4 nanoparticles, a novel magnetic flocculant, PCNF, was developed by employing Fe_3O_4 as the magnetic core and incorporating the adhesive properties of CMC and the coagulation efficacy of PFS to combine the advantages of magnetic separation with the synergistic effects of the functional components.

As shown in Fig. 10.(a), PCNF prepared with different mass ratios exhibited distinct flux decline behaviors during the coagulation-ultrafiltration process for high-algae water treatment. In the absence of a magnetic field, the specific flux achieved with the conventional coagulant PFS decreased to 0.78115, while that obtained with the novel flocculant PCNF at the optimal mass ratio of 1:1:3 reached 0.86154. The performance advantages of the optimal PCNF flocculant were further confirmed by comparing Fig. 10.(b) and(c). Using this flocculant resulted in a water flux decline rate of 20% and a UV_{254} removal efficiency of 65%, both superior to those observed for PFS (40% and 59%, respectively); furthermore, the flux recovery rate reached 85%, also higher than that achieved with PFS (78%). These improvements were attributed to the loose and porous cake layer formed by PCNF, which effectively retained small-molecule pollutants, reduced irreversible fouling, and thereby enhanced membrane cleaning efficiency.

Upon the introduction of an external magnetic field (Fig. 10d–f), the PCNF-coupled system exhibited a specific flux of 0.82523 at the end of the third cycle, surpassing both the magnetic field-free PCNF (0.80912) and PFS (0.74167) treatment systems; furthermore, the UV_{254} removal efficiency increased to 68%, outperforming the other two systems (65%, 59%). Fouling composition analysis revealed that treatment using PFS exhibited total, irreversible, and reversible fouling ratios of 88%, 25%, and 63%, respectively. Under magnetic field-free conditions, employing PCNF reduced these values to 80%, 19%, and 61%. In the presence of a magnetic field, total and irreversible fouling further decreased to 69% and 11%, while the flux recovery rate reached 89%. Compared with our previous membrane modification-only study [48] (flux recovery rate: 84%; irreversible fouling: 16%; UV_{254} rejection: 45%), the integrated process demonstrated significant improvements across all metrics, confirming that the synergistic combination of magnetic flocculation and magnetic field regulation optimized the cake layer structure, thereby enhancing organic matter retention and antifouling performance.

4. Discussion

4.1. Membrane fouling fitting of SPDA@MIL-101/PES mixed matrix membranes

To investigate the antifouling properties of ultrafiltration membranes, four classical fouling models (complete blocking, standard blocking, intermediate blocking, and cake filtration models) were employed to analyze the flux decline during algae-laden water treatment by M0 and M2 membranes (Fig. 11). The unmodified M0 membrane exhibited high goodness-of-fit values in the standard blocking (R^2 = 0.997), intermediate blocking (R^2 = 0.959), and cake filtration models (R^2 = 0.996), indicating a combination of fouling mechanisms. In contrast, the modified M2 membrane showed generally reduced fitting accuracy across all models, whereby the R^2 value of the standard blocking model decreased from 0.997 to 0.985, demonstrating significantly enhanced resistance to pollutant adsorption and pore blockage. Notably, the cake filtration model maintained a relatively high R^2 value (0.989), revealing that the formation of dense cake layers by algal cells and their secretions remained the primary fouling mechanism for both membranes.

Table 4 lists the R^2 values of fitting various fouling models to the filtration data obtained with different membranes. These values were

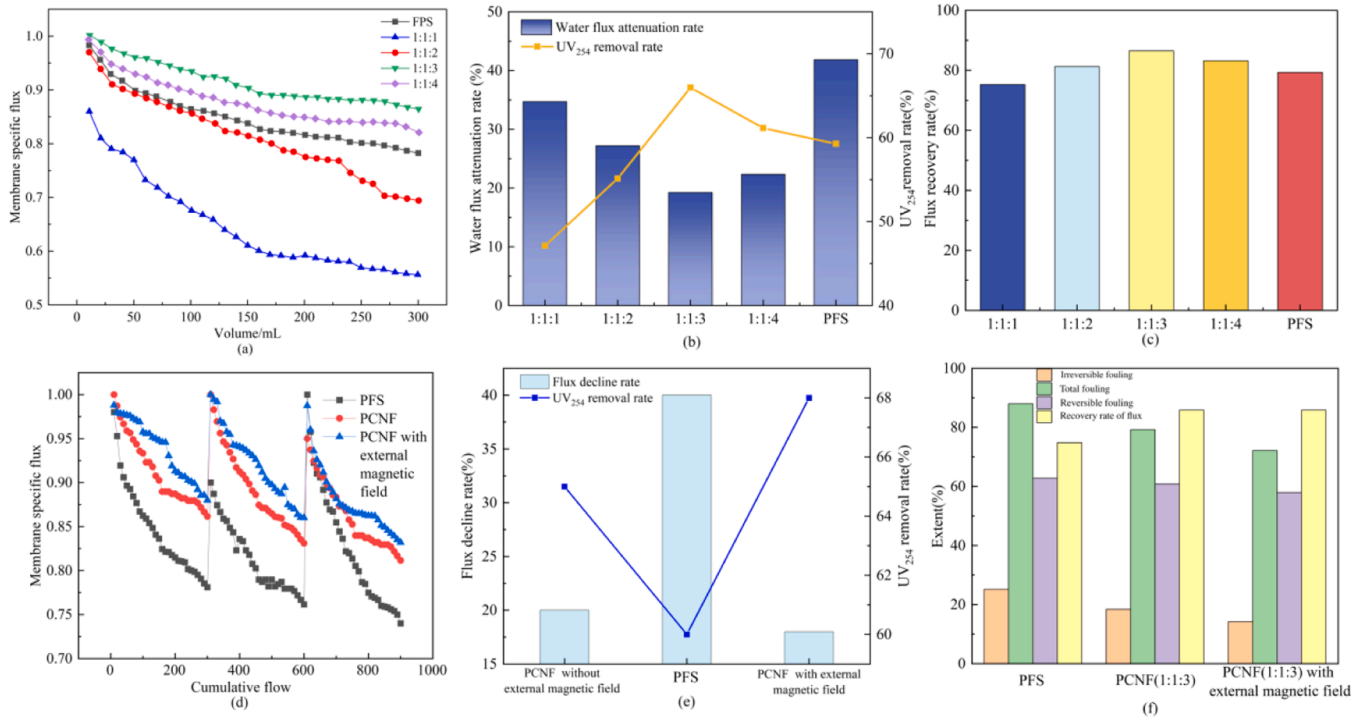


Fig. 10. Performance of novel membrane materials coupled with magnetic flocculation in high-algae water treatment.

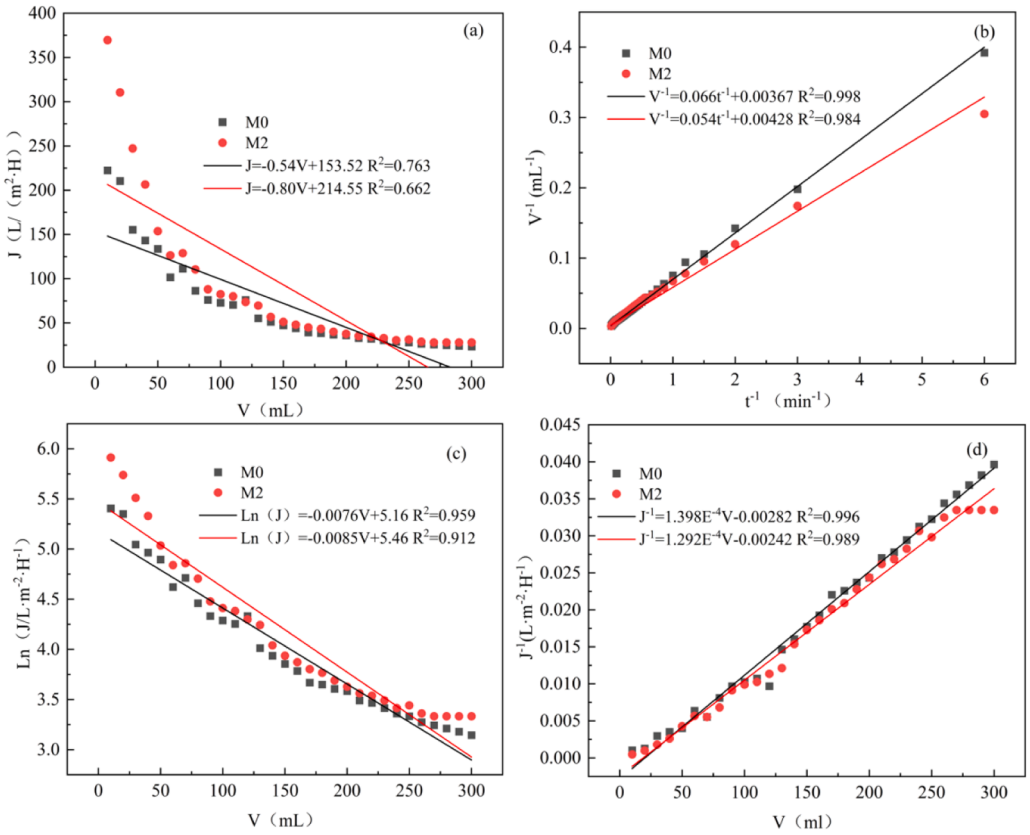


Fig. 11. Fitting of four fouling models in high-algae water treatment by M0 and M2 membranes: (a) Complete blocking model; (b) Standard blocking model; (c) Intermediate blocking model; (d) Cake layer model.

0.763 (complete blocking), 0.997 (standard blocking), 0.959 (intermediate blocking), and 0.996 (cake filtration) for the M0 membrane, indicating a combination of fouling mechanisms during algae-laden water filtration. Standard blocking, intermediate blocking, and cake filtration were identified as the dominant mechanisms, consistent with the observed reversible and irreversible fouling phenomena in the ultrafiltration process. With nanoparticle incorporation, the variation in R^2 values for the standard blocking and cake filtration models correlated closely with membrane hydrophilicity and antifouling performance, demonstrating that the modified membranes effectively alleviated standard blocking caused by small molecules and cake layer formation induced by algal secretions.

4.2. *Magnetic flocculation and structural analysis of the cake layer*

Fig. 12 presents the EDS elemental analysis results of the filter cake layers formed when applying PFS and PCNF, providing crucial insights into their pollutant retention mechanisms. Compared to the conventional flocculant PFS, the PCNF cake layer exhibited a significantly higher Fe content, indicating enhanced Fe loading in the novel composite flocculant, resulting in superior flocculation performance. Notably, under an applied magnetic field, the distributions of Fe and O elements became more homogeneous within the cake layer. This uniformity not only reflected the directional migration characteristics of magnetic flocculants under magnetic guidance but also demonstrated the capability of magnetic regulation to optimize the spatial distribution of flocculants, thereby enabling a more precise control over pre-loaded water samples. The optimized distribution ultimately resulted in a more porous and loose cake layer structure (as shown in Fig. 12), significantly improving both retention efficiency and permeation performance.

Furthermore, the distribution characteristics of Na elements provided additional insights into the compositional features of the PCNF composite flocculant. As a key component of CMC-Na, the uniform Na distribution indicated excellent dispersibility and binding capability of CMC-Na within the flocculant. This homogeneous distribution not only reflected the well-dispersed state of CMC-Na in the PCNF composite but also confirmed its crucial role in maintaining structural stability during cake layer formation.

Fig. 13 illustrates the morphological characteristics of filter cake layers formed by PFS and PCNF. Surface and cross-sectional SEM images revealed that the flocs generated from pre-loaded flocculated water had larger particle sizes and formed a pre-deposited floc layer with hierarchical porous structure after loading onto the ultrafiltration membrane. The cake layer displayed a loose and porous overall characteristic, exhibiting abundant pore structures, large specific surface area, and uneven surface topography with rough morphological features. Notably, cracks of varying widths were observed at the bottom regions of different cake layers, which may be related to the deposition process and structural stability of flocs on the membrane surface.

Compared to the PFS cake layer, the PCNF-formed pre-deposited floc layer demonstrated significantly enhanced porosity. This structural advantage provided a higher water flux and greater adsorption surface

Table 4
Fitting results of the four fouling models for high-algae water treatment by various membranes.

Membrane	Complete blockage model	Standard blockage model	Intermediate blockage model	Cake layer blockage model
M0	0.763	0.998	0.959	0.996
M1	0.632	0.991	0.888	0.991
M2	0.662	0.984	0.912	0.989
M3	0.675	0.989	0.910	0.994
M4	0.720	0.996	0.925	0.995

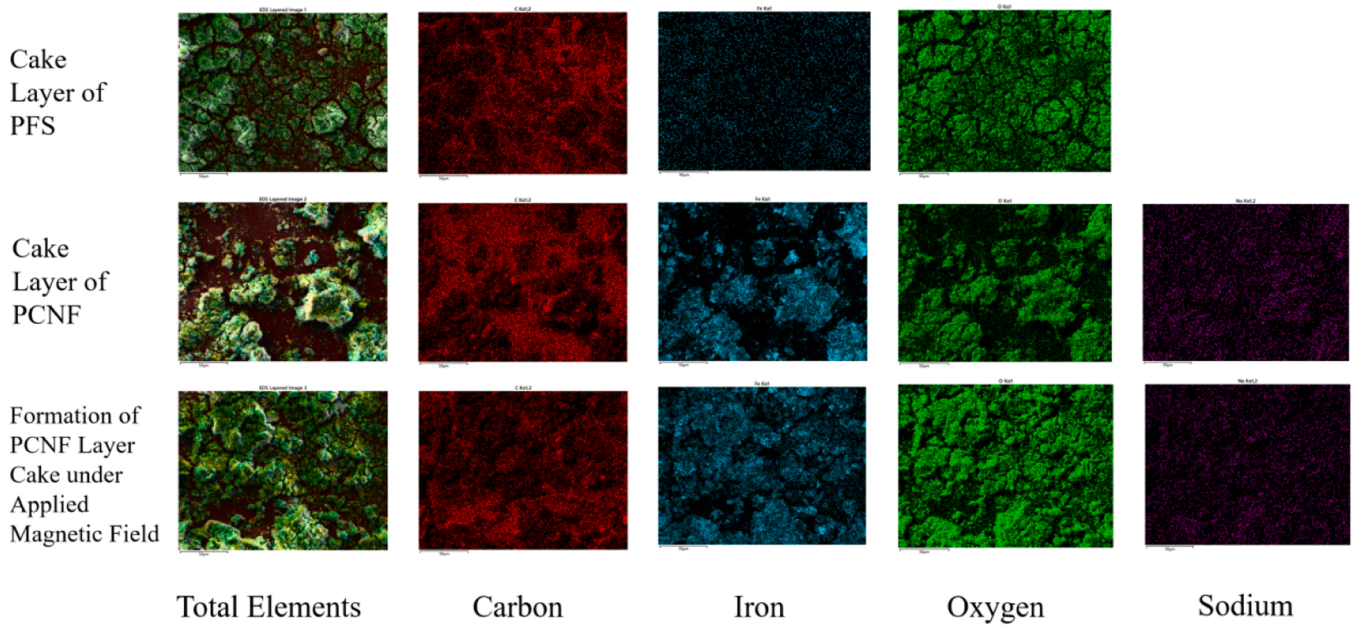


Fig. 12. EDS elemental composition analysis results of the cake layer obtained for various treatment systems.

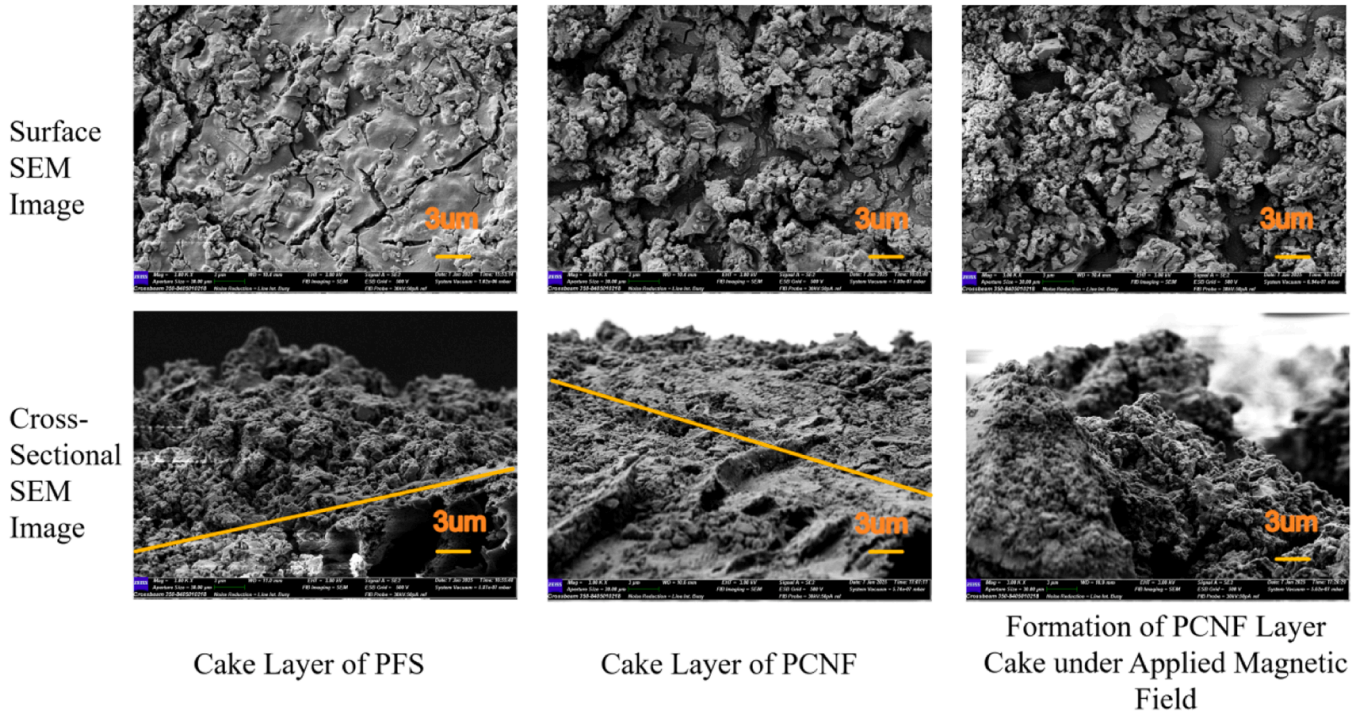


Fig. 13. SEM images of the cake layers obtained with various treatment systems.

area. More importantly, the loose and porous structure of the PCNF cake layer can effectively prevent pollutant penetration into membrane pores while significantly improving the removal efficiency of soluble organic matter. This performance enhancement was primarily attributed to the superior flocculation capability of PCNF and its optimization effect on the cake layer structure.

Under an applied magnetic field, the morphology of the cake layer on the ultrafiltration membrane surface showed remarkable improvements, presenting a more porous and uniform structure. This observation indicated that the magnetic-seeded PCNF flocculant enabled active optimization of cake layer morphology through magnetic field regulation, forming a structure with a porosity gradient. While maintaining the porous characteristics of the PCNF cake layer, this structure further optimized pore distribution through the oriented arrangement of magnetic particles, thereby enhancing pollutant retention capacity while significantly mitigating membrane fouling. Compared to non-magnetic conditions, the magnetic field-regulated cake layer structure demonstrated superior optimization, assuring efficient pollutant retention and long-term membrane fouling control.

4.3. Analysis of the coupling mechanism between novel membrane materials and magnetic flocculation for mitigating ultrafiltration membrane fouling in high-algal water treatment

As illustrated in Fig. 14, based on the experimental results and data analysis, this study proposes an "active magnetic field-mediated filter cake regulation" strategy for mitigating ultrafiltration membrane fouling in algae-laden water treatment through coupling novel membrane materials with magnetic flocculants under magnetic field conditions. A synergistic system integrating magnetic frameworks with gradient magnetic fields was constructed, providing a novel research paradigm for addressing membrane fouling problems. Specifically, during the coagulation phase, the magneto-fluidic coupling effect induces size-based gradation of magnetic flocs after adding magnetic coagulants, forming magnetically responsive flocculation units with controlled size distribution. During the filtration stage, the synergistic action of the gradient magnetic field and gravitational settling further optimizes the deposition process: larger flocs preferentially settle to form a porous skeletal base, while medium and small flocs progressively construct a dense top barrier. Through the precise control of magnetic field distribution, prioritized sedimentation of large flocs and directional stacking of small particles are achieved, ultimately forming a reverse-gradient structure characterized by a "porous bottom-dense top" configuration on the ultrafiltration membrane surface. This structural reorganization of the filter cake pore network not only enhances the retention efficiency of algal pollutants but also maintains high flux recovery rates.

To elucidate the intrinsic mechanism of dynamic filter cake reconstruction, a multiscale correlation model between magnetic field intensity, pore network, and mass transfer efficiency was established. Through magnetic parameter regulation, synergistic optimization was achieved, where highly porous structures at the cake layer bottom ensured flux maintenance while dense top structures enhanced pollutant rejection. This breakthrough successfully accomplishes the transition from "static accumulation" to "dynamic reconstruction" of filter cakes, providing theoretical support and technical assurance for ultrafiltration processes in the treatment of algae-laden water. Compared to conventional processes, the proposed magnetic field-mediated regulation strategy maintains the existing process framework while effectively balancing the contradiction between rejection efficiency and permeate flux, offering a solution with both theoretical innovation and engineering applicability for algae-laden water treatment. This achievement not only expands the application potential of magnetic flocculants in water treatment but also lays a crucial foundation for developing intelligent and dynamic membrane fouling control technologies.

5. Conclusion

This study established a synergistic "membrane material–flocculant–magnetic field regulation" process, providing a solution with both theoretical innovation and engineering feasibility for the treatment of algae-laden water. The main conclusions are as follows:

1. A SPDA@MIL-101/PES mixed matrix ultrafiltration membrane was successfully fabricated. The SPDA modification significantly improved the dispersion and compatibility of MIL-101 within the polymer matrix, providing the membrane with enhanced hydrophilicity, high electronegativity, and an interconnected pore structure, thereby significantly improving its contaminant retention capacity.
2. A novel magnetic flocculant, PCNF, with a Fe_3O_4:CMC-Na:PFS mass ratio of 1:1:3, was developed. Under an external magnetic field, this flocculant facilitated the formation of a cake layer with an axially graded structure, increased the proportion of reversible fouling, and achieved a high flux recovery rate of 89%.
3. A mechanism of magnetic field-mediated dynamic cake layer regulation was proposed. This mechanism optimizes the internal pore network of the cake layer by enabling the oriented arrangement and graded deposition of magnetic flocs, effectively overcoming the trade-off between contaminant retention and permeate flux in traditional treatment systems.

CRediT authorship contribution statement

Xiaoqing Dong: Resources, Funding acquisition, Data curation. **Zhilin Ran:** Funding acquisition, Formal analysis, Data curation. **Ting Chen:** Methodology, Investigation, Funding acquisition. **Ruiyan Xiang:** Methodology. **Ang Li:** Writing – original draft, Visualization, Validation, Investigation, Formal analysis, Data curation, Conceptualization. **Meng Yao:** Formal analysis, Data curation, Conceptualization. **Gang Liu:**

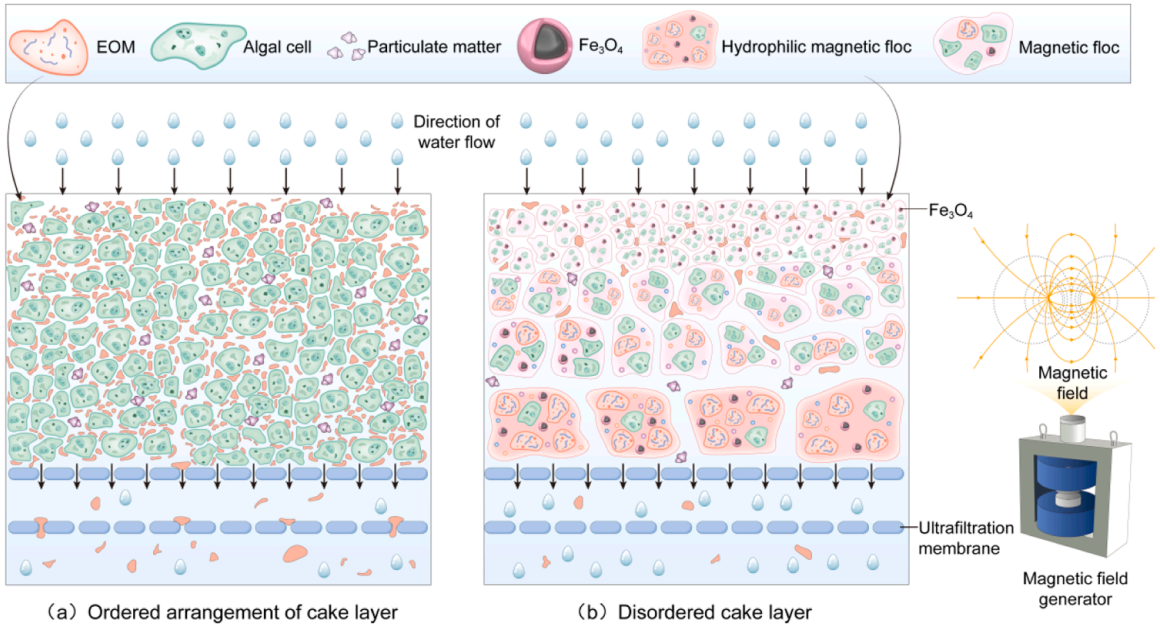


Fig. 14. Schematic diagram of the mechanism for mitigating ultrafiltration membrane fouling in high-algae water using novel membrane materials coupled with flocculation in the absence (a) and presence (b) of a magnetic field.

Writing – review & editing, Validation, Supervision.

Declaration of Competing Interest

The authors declare that they have no known competing financial interests or personal relationships that could have appeared to influence the work reported in this paper.

Acknowledgements

This work was supported by the National Natural Science Foundation of China (52500008), the Guangdong Province Ordinary University Innovation Team Project (2024KCXTD063), University-level Key Research Areas Support Projects (SZIIT2024KJ034), the Key Project of the Liaoning Provincial Department of Education (LJ212410153008), and the Shenzhen Key Industry R&D Program Major Project (ZDCYKCX20250901093303005).

Data availability

No data was used for the research described in the article.

References

[1] T. Li, Y. Wang, J. Zheng, et al., Singlet oxygen treatment of algae-laden water: an elegant way of decontamination without cellular damage[J], Water Res. 283 (2025) 123892.
[2] N. Suryakant, G. Sashi, Q. Qi, et al., Cyanotoxins increase cytotoxicity and promote nonalcoholic fatty liver disease progression by enhancing cell steatosis.[J], Toxins 15 (7) (2023).
[3] X. Qiu, Z. Liu, X. Li, et al., Contribution of specific extracellular organic matter on membrane fouling in ultrafiltration and coagulation-ultrafiltration of algae-laden water[J], Int. Biodeterior. & Biodegrad. 196 (2025) 105932.
[4] R. Zhijun, W. Siyang, W. Qiuwen, et al., Moderate KMnO4/Fe(II) pre-oxidation for membrane fouling mitigation in algae-laden water treatment[J], Sep. Purif. Technol. 314 (2023).
[5] X. Cheng, J. Lian, B. Liu, et al., Integrated ferrate and calcium sulfite to treat algae-laden water for controlling ultrafiltration membrane fouling: high-efficiency oxidation and simultaneous cell integrity maintaining[J], Chem. Eng. J. 461 (2023) 141880.
[6] L. Jinchuan, Z. Lijie, T. Fengxun, et al., Enhancing ultrafiltration of algal-rich water using ferrate activated with sodium percarbonate: foulants variation, membrane fouling alleviation, and collaborative mechanism.[J], Chemosphere 308 (P2) (2022) 136377.
[7] S. Babel, S. Takizawa, Microfiltration membrane fouling and cake behavior during algal filtration[J], Desalination 261 (1) (2010) 46–51.
[8] F. Qu, H. Liang, J. Tian, et al., Ultrafiltration (UF) membrane fouling caused by cyanobateria: fouling effects of cells and extracellular organics matter (EOM)[J], Desalination 293 (2012) 30–37.
[9] L.O. Villacorte, Y. Ekowati, H. Winters, et al., MF/UF rejection and fouling potential of algal organic matter from bloom-forming marine and freshwater algae [J], Desalination 367 (2015) 1–10.
[10] V. Discart, M.R. Bilad, D. Vandamme, et al., Role of transparent exopolymeric particles in membrane fouling: chlorella vulgaris broth filtration[J], Bioresour. Technol. 129 (2013) 18–25.
[11] S. Li, X. Wang, Y. Guo, et al., Recent advances on cellulose-based nanofiltration membranes and their applications in drinking water purification: a review[J], J. Clean. Prod. 333 (2022) 130171.
[12] A. Yusuf, A. Sodiq, A. Giwa, et al., A review of emerging trends in membrane science and technology for sustainable water treatment[J], J. Clean. Prod. 266 (2020) 121867.
[13] G. Wang, G. Xu, Construction of superhydrophobic MOF membrane for ultrafast alcohol-water separation[J], Sci. Bull. 67 (23) (2022) 2381–2383.
[14] X. Shao, G. Yao, Z. Wang, et al., MOFs and surface modification synergistically modulated cellulose membranes for enhanced water permeability and efficient tellurium separation in wastewater[J], J. Clean. Prod. 434 (2024) 139873.
[15] Y. Sun, J. Yan, J. Jiang, et al., Hierarchical defect-rich UiO-66 membrane towards superior flue gas and butane isomer separations[J], Sci. Bull. 69 (14) (2024) 2174–2178.
[16] K. Mohammed, A. Mustafa, S. Suhaib, et al., A review on UiO-66 applications in membrane-based water treatment processes[J], J. Water Process Eng. 51 (2023).
[17] W. Yi, L. Daxue, L. Jian, et al., Metal organic framework UiO-66 incorporated ultrafiltration membranes for simultaneous organic matter and heavy metal ions removal.[J], Environ. Res. 208 (2022) 112651.
[18] J. Farahbakhsh, M. Golgoli, M. Najafi, et al., An innovative NH2-UiO-66/NH2-MIL-125 MOF-on-MOF structure to improve the performance and antifouling properties of ultrafiltration membranes[J], Sep. Purif. Technol. 353 (PA) (2025) 128273.
[19] D. Mona, M. Toraj, M.M. Tavakol, et al., Metal-organic framework/zeolite nanocrystal/polyvinylidene fluoride composite ultrafiltration membranes with flux/antifouling advantages[J], Mater. Chem. Phys. 260 (2021).
[20] S. Mahya, Z. Sirus, Z.A. Akbar, et al., A new antifouling metal-organic framework based UF membrane for oil-water separation: a comparative study on the effect of MOF (UiO-66-NH2) ligand modification[J], Korean J. Chem. Eng. 39 (11) (2022) 3092–3101.
[21] T. Lan, J. Song, Y. Chang, et al., Bifunctionalized MOFs modified poly (aryl ether ketone sulfone) ultrafiltration membranes with high-efficient BSA separation and dye adsorption[J], J. Membr. Sci. 713 (2025) 123318.
[22] T. Lan, Y. Chang, J. Song, et al., Dual synergies of functionalized hydrophilic MOFs based poly (aryl ether ketone sulfone) ultrafiltration membranes: electrostatic action and pore size screening[J], J. Environ. Chem. Eng. 12 (5) (2024) 113788.
[23] R.S. Hebbar, A.M. Isloor, K. Ananda, et al., Fabrication of polydopamine functionalized halloysite nanotube/polyetherimide membranes for heavy metal removal[J], J. Mater. Chem. A (2016).
[24] D. Kadadou, T. Arumugham, L. Tizani, et al., Enhanced antifouling and separation capabilities of polydopamine@Ce-MOF functionalized PES ultrafiltration membrane[J], npj Clean. Water 7 (1) (2024) 7.
[25] Z. Xiaocan, W. Mengxin, L. Pinglin, et al., L-Cysteine functionalized halloysite nanotubes/PVDF ultrafiltration membrane for improving anti-fouling performance [J], J. Environ. Chem. Eng. 11 (6) (2023).
[26] K. Mithun, A. M. I, M.C. S. N, et al., Hydrophilic polydopamine/ polyvinylpyrrolidone blended polyphenylsulfone hollow fiber membranes for the removal of arsenic-V from water[J], J. Environ. Chem. Eng. 11 (5) (2023).
[27] Z. Chaoxu, W. Jin, Z. Qingyun, et al., Explication of polydopamine modified g-C3N4 as effective additive in PVDF nanocomposite membrane fabrication for enhanced ultrafiltration and self-cleaning performance[J], J. Environ. Chem. Eng. 11 (5) (2023).
[28] L. Fu, M. Li, L. Wang, et al., Effects of membrane fouling, cleaning, and aging on ultrafiltration performance in water treatment systems[J], J. Clean. Prod. 533 (2025) 147030.
[29] W. Yang, F. Zhou, J. Lee, et al., Understanding the fouling characteristics in ultrafiltration membrane for marine algae-laden seawater pretreatment: Focus on the role of algal extracellular organic matter[J], J. Clean. Prod. 479 (2024) 144084.
[30] Y. Yu, X. Feng, Y. Jian, et al., Mutual treatment of algae organic matters and heavy metal ions using a coagulation process: Processes and mechanisms[J], Sep. Purif. Technol. 362 (P3) (2025) 131900.
[31] S. Wang, S. Yang, H. Chen, et al., The Role of Ferrate (VI) in the Pretreatment of Algal Cells and Algal Organic Matters: A Review[J], Water 16 (10) (2024).
[32] J. Wang, J. Yang, H. Zhang, et al., Feasibility study on magnetic enhanced flocculation for mitigating membrane fouling[J], J. Ind. Eng. Chem. 26 (2015) 37–45.
[33] C. Yunxuan, N. Jun, A strategy to alleviate membrane fouling by optimizing the structure of the cake layer formed by flocs deposited directly on the membrane in the ultrafiltration process through coagulation and nanoscale Fe3O4/Fe3O4@SiO2 load[J], J. Membr. Sci. 680 (2023).
[34] M. Yao, X. Dong, Z. Ran, et al., Effect of nano Fe3O4-(CMC-Na)-PFS coagulant on coagulation–ultrafiltration process for treatment of algae -rich water[J], Desalin. Water Treat. 317 (2024) 100307.
[35] S. Jianxuan, Z. Jinhua, W. Chengze, et al., Research progress on the magnetite nanoparticles in the fields of water pollution control and detection.[J], Chemosphere 336 (2023) 139220.
[36] S. Jingjing, Y. Zhenjiang, Y. Libin, et al., New insight in algal cell adhesion and cake layer evolution in algal-related membrane processes: Size-fractioned particles, initial foulant seeds and EDEM simulation.[J], Environ. Res. 220 (2022) 115162.
[37] Q. Ye, C. Zhou, J. Hu, et al., Presence of iron oxide particles can reduce the cake fouling in UF systems[J], Sep. Purif. Technol. 342 (2024) 127015.
[38] Y. Xuesong, N. Jun, H. Xinhao, et al., Intensifying low-pressure membrane performance based on bio-cake layers coupled with pre-loading layers[J], J. Membr. Sci. 690 (2024).
[39] J. Pala, R. Tracy, S.N. Mahmoodi, et al., Real-time induced magnetic vibrational based antifouling mechanism for ultrafiltration (UF) membrane[J], J. Membr. Sci. 713 (2025) 123313.
[40] Z. Ali, S. Kiran, N.U. Haq, et al., Fabrication of novel (Cr) based (MIL-101) incorporated mixed matrix forward osmosis membranes for environmental remediation[J], Mater. Chem. Phys. 315 (2024) 128951.
[41] Y. Yahia, K.T. Rashid, M.A. Toma, et al., A novel green propolis (bee glue) nanoparticles mixed with poly (ether-sulfone) ultrafiltration membrane for wastewater Eriochrome Black T (EBT) and Congo Red (CR) dye treatment[J], J. Environ. Chem. Eng. 13 (2) (2025) 115913.
[42] F. Hassani, A. Aroujalian, A. Rashidi, Robust and stable superhydrophilic MIL-101 (Cr)-coated copper mesh for highly efficient oil/water emulsion separation.[J], Environ. Sci. Pollut. Res. Int. 31 (21) (2024) 30663–30675.
[43] I.H. Ahmad, J. Khairulazhar, S.N. Soraya, et al., Experimental and Modeling of Dicamba Adsorption in Aqueous Medium Using MIL-101(Cr) Metal-Organic Framework[J], Processes 9 (3) (2021) 419.
[44] T. S M, G. BonHyuk, P.S. Yane, et al., Nafion Composite Membranes Impregnated with Polydopamine and Poly(Sulfonated Dopamine) for High-Performance Proton Exchange Membranes.[J], ACS Omega 7 (15) (2022) 12956–12970.
[45] Y. Golabkesh, M.S. Fattahi, T. Mohammadi, A study on effect of stearic acid-modified cellulose nanocrystals on morphology and performance of PVDF membranes in vacuum membrane distillation[J], Sep. Purif. Technol. 382 (2026) 135961.

[46] Z. Liang, J. Wang, Q. Zhang, et al., Composite PVDF ultrafiltration membrane tailored by sandwich-like GO@UiO-66 nanoparticles for breaking the trade-off between permeability and selectivity[J], Sep. Purif. Technol. 276 (2021) 119308.
[47] Z. Hao, J. Chen, D. Zhang, et al., Coupling effects of Zn single atom and high curvature supports for improved performance of CO2 reduction[J], Sci. Bull. 66 (16) (2021) 1649–1658.
[48] M. Yao, Y. Li, Z. Ran, et al., Polydopamine-functionalized metal-organic framework nanomaterials for enhanced ultrafiltration membrane performance in high-algae water treatment[J], J. Environ. Chem. Eng. 13 (2) (2025) 115482.